Development of the UT San Antonio FLame and Advanced Rocket Experimentation (FLARE) test facility

Joseph Hernandez-McCloskey*†, Kevin M. Eisenbarger*, Krystal Corral Martinez*, Seth A. Reutlinger*, Justin Torbey*, Eshwar Saikumar‡, Victor Nagy‡, and Daniel I. Pineda§
The University of Texas at San Antonio (UT San Antonio), San Antonio, Texas, 78249

The FLame and Advanced Rocket Experimentation (FLARE) facility at The University of Texas at San Antonio was built to close the design–build–test–iterate (DBTI) cycle for metal additively manufactured (AM) propulsion hardware on a campus without existing test capability. Hardware validation—a required step in DBTI-driven AM development—demands a controlled hot fire test environment. FLARE was student-designed, student-sourced, and student-built to establish a robust testbed for research-grade rocket and air-breathing combustor development under tight resource constraints. The facility delivers up to 2 lb/s of stoichiometric gaseous methane–oxygen to support ∼500-lbf thrust-class combustors, including rotating detonation rocket engines (RDREs). The thrust stand structure sustains loads up to 1500 lbf with a factor of safety (FOS) of 4. Subsystems for propellant handling/metering, cooling, thrust measurement, data acquisition and control, and custom electronics were developed from first principles to meet accuracy, robustness, and safety requirements across extreme operating regimes in next-generation propulsion systems. The facility architecture reflects necessity-driven decisions: commercial turnkey systems were financially and operationally out of reach. FLARE instead employs repurposed industrial hardware, purchased components, and in-house-fabricated parts to support rapid DBTI cycle closure. This work documents the design logic, supporting analyses, fabrication approach, and current build status of the v0 FLARE facility as a framework for establishing propulsion test capability where commercial infrastructure is inaccessible and no heritage facilities exist. Beyond its immediate research goals, FLARE demonstrates end-to-end, student-led execution across mechanical design, manufacturing, and integration of safety-critical systems: capabilities required for new entrants to develop advanced propulsion hardware in the New Space era.

I. Nomenclature

$\dot{m}$ = mass flow rate
ϕ = equivalence ratio
P = pressure
T = temperature

II. Introduction

Metal additive manufacturing has transformed the development of next-generation propulsion hardware. It enables physics-driven geometry tailoring, reduces process scrap/waste [1], and unlocks compact, high-heat-flux systems like rotating detonation rocket engines (RDREs) [2]. To realize these systems at New Space pace, teams must rapidly close the design-built-test-iterate (DBTI) cycle; hardware maturation, life evaluation [3], and physics-based model development/validation [4] demand full component lifecycle visibility. While AM allows rapid production of actively cooled components—hardware historically inaccessible to universities—the DBTI cycle often stalls immediately after manufacture; without in-house test infrastructure, these systems cannot be proven through fire.

*Graduate Research Assistant, Department of Mechanical, Aerospace, and Industrial Engineering, AIAA Student Member
†NASA Space Technology Graduate Research Opportunities (NSTGRO) Fellow, Engine Components and Technology Branch
‡Undergraduate Research Assistant, Department of Mechanical, Aerospace, and Industrial Engineering, AIAA Student Member
§Associate Professor, Department of Mechanical, Aerospace, and Industrial Engineering, AIAA Member

Since 2021, the University of Texas at San Antonio (UT San Antonio) has expanded its role in propulsion research through collaborations with NASA Marshall Space Flight Center (MSFC) [4], the Air Force Research Laboratory (AFRL) [5–7], and internal programs [8–10]: a growing internal propulsion portfolio. Through recent investment by UT San Antonio as well as research projects sponsored by federal agencies targeting domestic graduate student workforce development, students now design and fabricate AM combustors, rocket torch igniters, and propulsion systems across multiple thrust classes spanning 1-lbf to 500-lbf. Each component is built for sustained, steady-state operation.

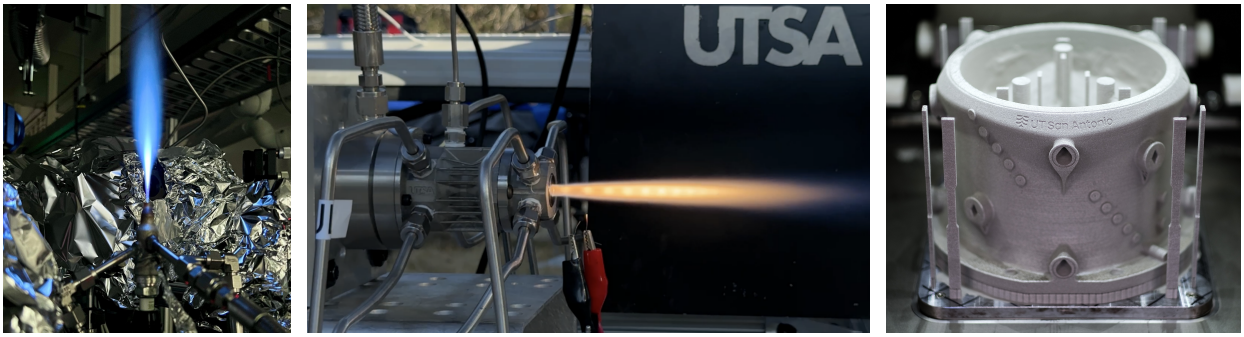

Fig. 1 UT San Antonio AM propulsion hardware development capabilities, 2023–2025

While in-house AM capability and over 6000 seconds of laboratory torch operation have been proven, UT San Antonio lacked a dedicated test environment to evaluate these components under flight-realistic conditions. Furthermore, external facilities could not meet realistic research timelines, safety/instrumentation requirements, or flexible configuration needs; external reliance for UT San Antonio propulsion advancement was considered unjustifiable and antithetical to the university's core missions, which include being an innovative place to work, learn, and discover. An internal testbed for student-developed propulsion hardware became essential; hands-on student ownership of the hardware lifecycle was deemed paramount for program longevity, research output, and future New Space workforce development.

The FLame and Advanced Rocket Experimentation (FLARE) facility was conceived, developed, and is being built by students to establish in-house test infrastructure and enable full DBTI cycle closure on the UT San Antonio campus. FLARE's architecture, subsystem design, and operations methodology were shaped by necessity; students required research-grade test capability without access to turnkey commercial systems or heritage infrastructure. This work outlines the design logic, integration strategy, and current build status of the v0 FLARE facility: a replicable framework to establish research-grade propulsion test capability in resource-constrained environments.

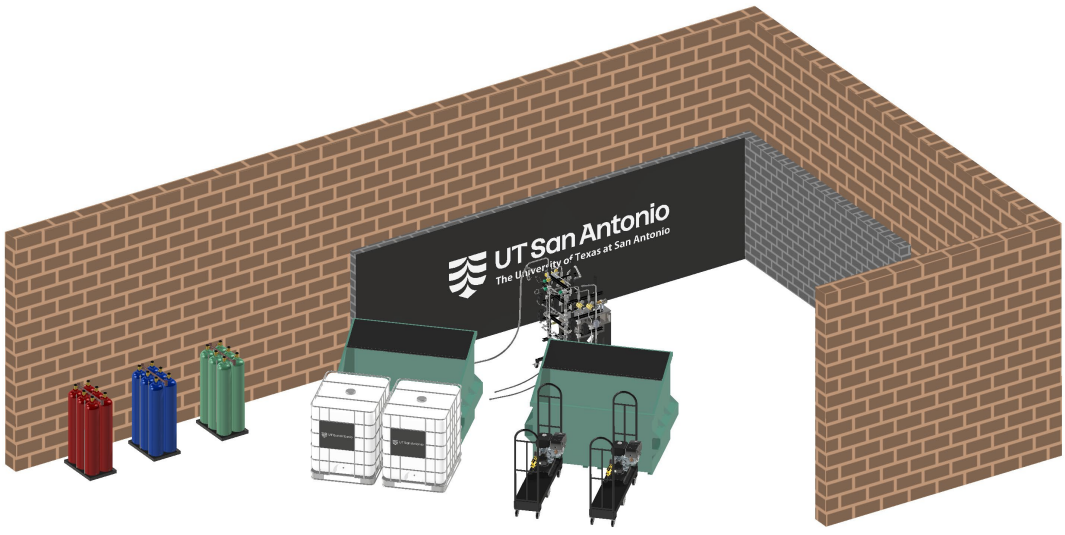

Fig. 2 CAD render of UT San Antonio FLARE facility

III. Methods

The v0 FLARE facility design was driven by system-level performance requirements; target operating conditions, research hardware scale, safety constraints, on-site manufacturing capabilities, and a rapid design-build-test-iterate (DBTI) cadence directly shaped the facility architecture. The resulting system integrates propellant handling, thrust measurement, cooling, ignition, and data acquisition/control through the requirements-driven workflow defined in Table 1. Acronyms used in the facility requirements table include: gCH_4/gO_2 (gaseous methane–oxygen), CFV (critical flow venturi), TA (test article), DAQ (data acquisition), EMI (electromagnetic interference), cRIO (compact RIO controller), PCB (printed circuit board), and COTS (commercial-off-the-shelf).

Table 1 v0 FLARE Facility Requirements and Design Implications

ID	Requirement	Design Implication
R-1	Deliver up to 2 lb/s of stoichiometric gCH_4/gO_2	Sets the ~500-lbf TA envelope; dictates regulator Cv, CFV sizing, and line diameter.
R-2	Support TA pressures up to 1000 psig without CFV unchoking	Constrains allowable line losses, valve Cv, and CFV backpressure margin.
R-3	Withstand 1500 lbf thrust with FOS ≥ 4	Informs flexure geometry, weld process, and load cell interface.
R-4	Provide ≥ 4 lb/s coolant flow at TA-compatible pressures	Drives pump selection, routing strategy, and pressure drop allowance.
R-5	Enable safe sequencing and rapid abort capability	Governs relay logic, interlocks, and test redline enforcement.
R-6	Synchronously acquire thrust, pressure, and temp at >2 kHz	Sets cRIO module specifications, buffer architecture, and control method.
R-7	Maintain signal integrity against EMI and ignition events	Enforces grounding layout, cable shielding, and PCB design.
R-8	Support hardware reconfiguration in <1 hour	Dictates top plate layout, interface geometry, and mounting scheme.
R-9	Be fully manufacturable and maintainable in-house	Frames fabrication approach, tooling needs, and design-for-maintenance.
R-10	Remain within project-allocated budget constraints	Limits COTS reliance, outsourcing scope, and v0 hardware ambition.

A. System Architecture Overview

The v0 build of the UT San Antonio FLARE facility is sized to support up to 2 lb/s of stoichiometric gCH_4/gO_2 propellants with corresponding test article (TA) pressures up to 1000 psig. This flow capability enables hot fire test of ~500-lbf research combustors and directly aligns with subscale test articles used at NASA MSFC (i.e., TC-105 [11]), and AFRL-EAFB (i.e., EC-1 [12]). These high-level system definitions drive requirements for pressure drops, flow metering, valve selection, coolant flow capability, thrust structure design, and low-speed instrumentation bandwidth. Visualization of subscale RDRE hardware created in collaboration with NASA at the 500-lbf thrust class is shown in Fig. 3 at NASA MSFC TC-105.

A secondary "B-configuration" of FLARE, which incorporates a large-bore pressure regulator for air, supports hot fire testing at up to ~2.5 lb/s for stoichiometric ethylene-air and hydrogen-air mixtures. The configuration is critical for validating in-house-developed air-breathing RDEs, where air serves as the oxidizer [7]. The dual-mode FLARE architecture enables both rocket and air-breathing detonation engine research alongside AM deflagration engine development at UT San Antonio; it supports full DBTI cycle closure across propulsion subdomains.

Initial hot fire testing will be conducted with in-house additively manufactured actively cooled deflagration-based rocket hardware to de-risk facility operations prior to RDRE campaigns. Subsequent test efforts—with hardware like that shown in Fig. 3 and UT San Antonio-developed air-breathing RDE configurations—will investigate detonative heat transfer, thermochemistry, combustor operating physics, and material survivability under extreme conditions. Methane

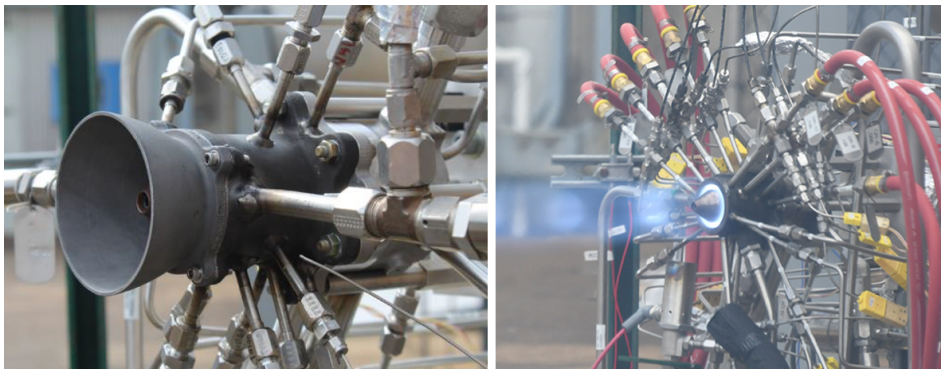

Fig. 3 Scale of hardware to be tested at UT San Antonio: subscale RDRE testing at NASA MSFC *left* from [11], hot fire *right* from [4]

was selected as the initial fuel for rocket-based studies to align with NASA's Moon-to-Mars Architecture goals [13, 14] as well as narrow range of flammability limits (relative to hydrogen) for reduced-risk system checkouts and initial testing. Additionally, gaseous propellant states are used to enable direct comparison with publicly available literature [15]. Full integration and initial hot fire test are planned for early 2026. The next subsections detail each of the FLARE subsystems.

B. Fluid Systems

Both high-flow and high-pressure capabilities were desired for research-relevant combustor operation within FLARE. High-flow is desired for increased thrust levels, and high pressure is desired to evaluate the effects of heightened thermal/structural loads on actively cooled hardware. The CAD model of the propellant fluid system is shown in Fig. 4.

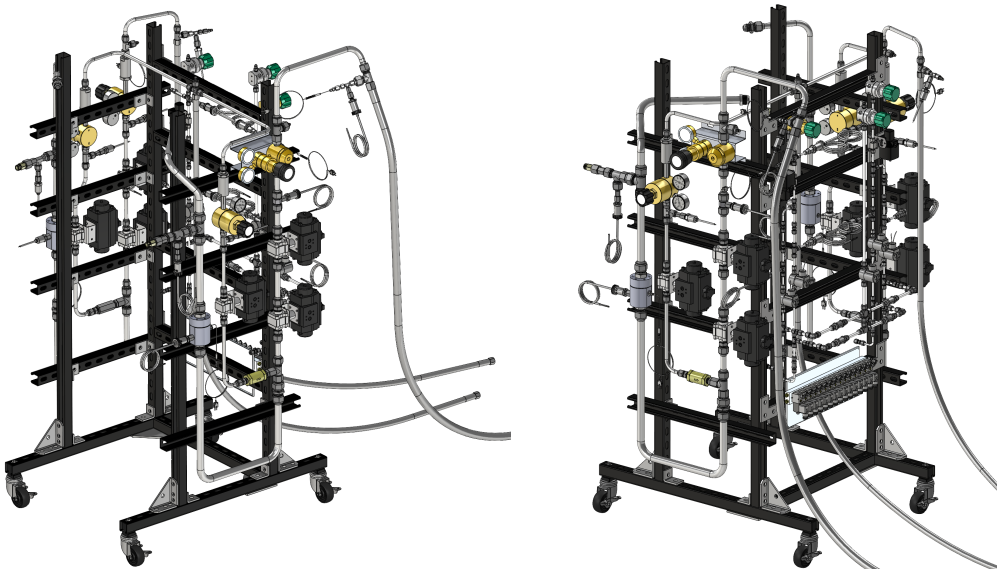

Fig. 4 FLARE propellant fluid system CAD render

The flow system uses critical flow venturis (CFV) [16], also referred to as sonic nozzles (SN) [17] to regulate the propellant mass flow rates. Sonic nozzles are used instead of choked orifices to enable a larger window of downstream pressures before unchoking; the diffuser section in CFVs enables pressure recovery which allows for higher maximum back pressure ratios (MBPR) and thus higher test article pressures for a given upstream pressure budget. Pressure and temperature are measured upstream of the sonic nozzles in accordance with the ASME MFC-7 standard to determine the upstream density and set the thermodynamic state for mass flow calculation. Fig. 5 illustrates the v0 plumbing and instrumentation (P&ID) diagram for the test stand.

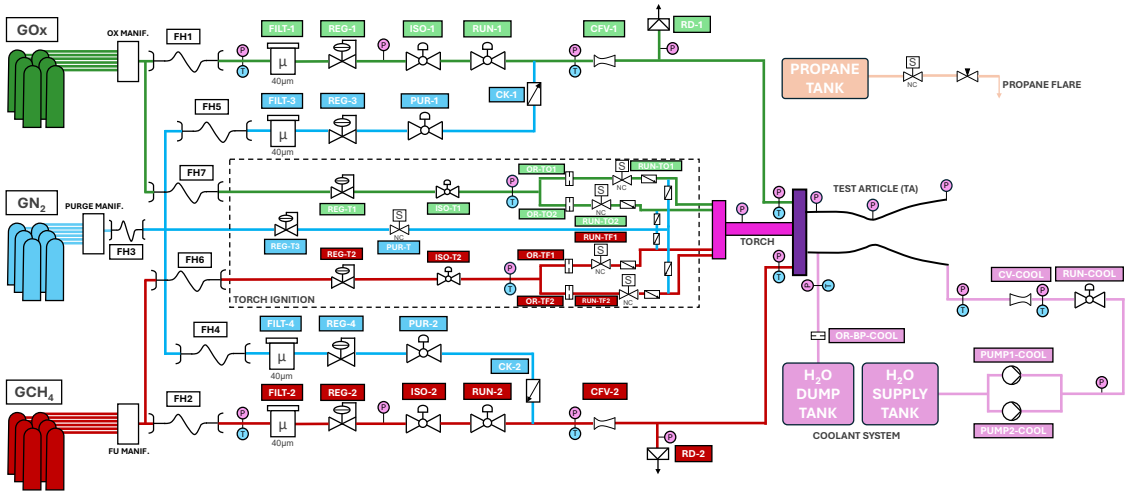

Fig. 5 UT San Antonio V0 FLARE facility plumbing and instrumentation diagram (P&ID)

Pneumatically-actuated ball valves are used instead of solenoid valves for main propellant valves (isolation and run). Large flow coefficients (Cv) were desired to minimize total pressure loss in the system, enabling more headroom for available chamber pressures, and also featured slower open/closure times to minimize pressure transients. Through this configuration, the flow system can support 1000 psig chamber pressures without unchoking the sonic nozzles. The NASA Generalized Fluid System Simulation Program (GFSSP) software [18] was used to validate flow velocities throughout the system were below 100 ft/s at maximum v0 flow conditions [19].

Test articles are cooled through two gasoline-powered pressure washer pumps, connected in parallel, to achieve a total of ~ 4 lb/s water coolant flow. A small supply of this water is diverted for pad flush.

Propellant ignition is achieved through an in-house developed AM torch igniter, pictured in Fig 1. A torch-style design is employed to successfully ignite propellants; flameholding is difficult within the chamber in the presence of high-velocity injected propellants: the common "match in hurricane" analogy. Furthermore, the torch design is favored for harder-to-ignite propellants (like methane) which would otherwise be difficult to ignite via Nichrome wire resistance heating (or even back-lighting with exit-plane propane flare). Valves were procured through eBay and inspected, tested, rebuilt, and/or oxygen-cleaned before being qualified for service. The current status of fluid system infrastructure is shown and dsecribed in Fig. 6

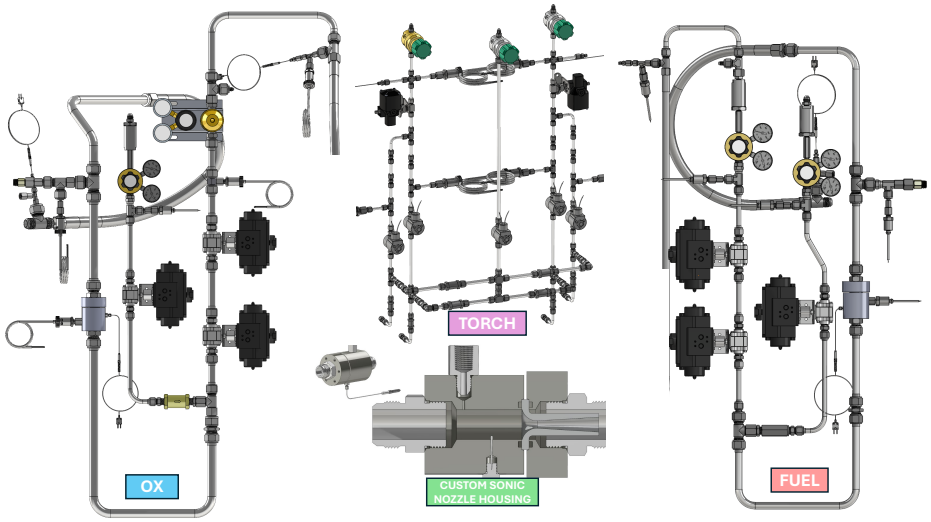

Fig. 6 FLARE propellant fluid systems for Ox *(left)*, Fuel *(right)*, Torch Ignition *(center)*, and a custom design for a Sonic Nozzle housing traceable to ASME MFC-7 *(bottom)*

C. Test Stand Structure

1. Design Rationale

The test stand was designed to provide accurate, repeatable thrust measurements for research-scale propulsion devices while maintaining structural integrity, modularity, and mobility. The primary design objective was to support thrust levels up to 1500 lbf, at a factor of safety (FOS) of 4. A modular design was implemented to allow rapid reconfiguration for different experimental setups including deflagration and detonation engines, thrust classes, load cell styles, and accommodation for different diagnostics like laser absorption spectroscopy (LAS). The fixture table is mechanically isolated from the base structure using a flexure system, ensuring that applied thrust loads are transmitted directly into the measurement load cell while minimizing parasitic loads from stand compliance, friction, or misalignment.

Material selection was driven by manufacturability, structural performance, durability, and cost. The base structure and anchoring system were fabricated from low-carbon structural steels (A513 and A36), providing sufficient strength at reasonable cost and ease of fabrication. Surface finishes were selected to prevent corrosion and improve longevity, with industrial enamel coating applied to most of the carbon steel, with the exception of components that were bolted together which were instead coated with a water-based corrosion inhibitor. All stainless-steel components were left as-machined.

This design approach aligns with thrust stand architecture successfully implemented at multiple academic and government laboratories, emphasizing accuracy, reproducibility, and maintainability without introducing unnecessary complexity.

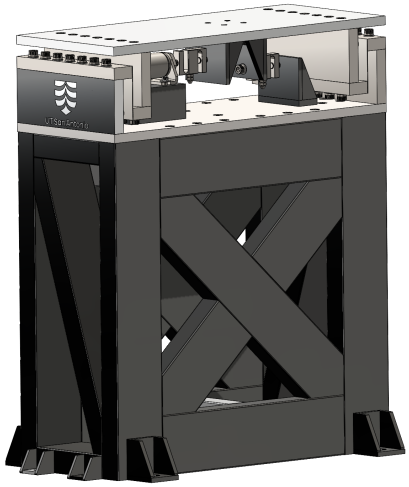

Fig. 7 UT San Antonio FLARE test stand structure CAD rendering, assembled.

2. Weld Parameter Design

High-quality welds and tight dimensional control were essential to ensure that the test stand could withstand high loads and repeated thermal-mechanical cycling generated by different propulsion devices. Gas Tungsten Arc Welding (GTAW), also known as TIG, was selected due to its superior control of heat input, arc stability, and highly tunable parameters. This welding method enabled precise, localized control of melt pools while minimizing the effects of warpage.

Welding parameters, summarized in Table 2, were developed to ensure repeatability and consistency across the numerous welded joints. When combined with joint preparation; including specifications for V-grooves and defined weld pass locations, seen in Fig. 8, a highly refined process contributed to exceptionally uniform, high-strength welds throughout the test stand.

Overall, the combined control of joint preparation and carefully developed welding parameters implemented with GTAW, resulted in structurally robust and consistent welding across the test stand. The effectiveness of this approach is illustrated by clearly defined root, filler, and cap passes shown in Fig. 9, which demonstrate proper fusion, penetration, and bead geometry achieved throughout fabrication. These results confirm that the process put forth met the structural requirements necessary for repeated high-load propulsion testing.

Weld Location	Pass Type	Filler	Filler Ø	Tungsten	Tungsten Ø	Cup Size	Current (A)
Single-V Butt Joint (1G)	Root, Fill, Cap	ER70S-2	3/32 in	EWTh-2	1/8 in	#8	210
Right-angle fillet (1F)	Root, Fill, Cap	ER70S-2	3/32 in	EWTh-2	1/8 in	#8	210
Inclined-angle fillet (1F)	Root, Fill, Cap	ER70S-2	3/32 in	EWTh-2	1/8 in	#8XL	210

Table 2 Welding parameters

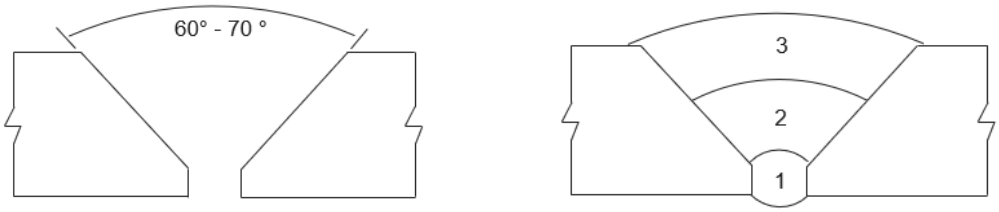

Fig. 8 Weld preparation *(left)*, Pass location *(right)*

Fig. 9 Root pass *(left)*, Fill pass *(middle)*, Cap pass *(right)*

3. Flexure System

A plate-style flexure system, as shown in Fig. 10, was implemented to guide thrust-induced motion along a single axis while constraining undesired degrees of freedom. Flexures are compliant structural elements that rely on elastic deformation rather than rolling or sliding motion, thereby eliminating stiction, friction, and backlash that can affect accuracy and repeatability. By isolating the load cell from off-axis forces, the flexure system improves measurement fidelity and reduces calibration drift. Flexure thickness was selected based on thrust class, with thicknesses ranging from 24 to 10 gauge stainless-steel sheet metal. Hand calculations and FEA, as shown in Fig. 10 were used to confirm that flexure deflections were sufficient to translate a thrust to the load cells, ensuring durability and consistent performance.

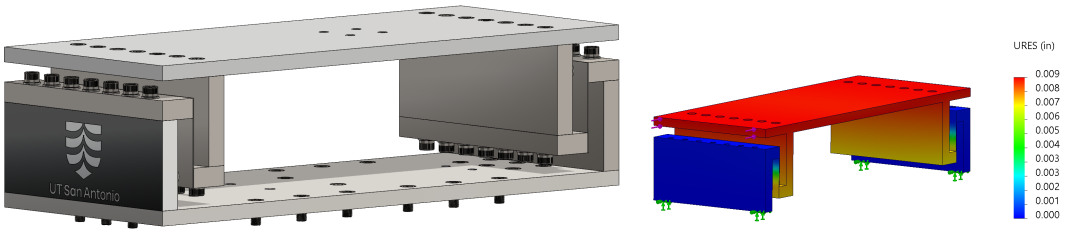

Fig. 10 Flexure defelction analysis

4. Calibration Load Cell

An independent calibration load cell system, as shown is Fig. 11, was developed to provide traceable verification of thrust measurement accuracy. The calibration approach applies a known force to the fixture table using a pneumatically actuated cylinder, where the applied force is determined from the product of regulated supply pressure and piston area. This method has been widely adopted at other institutions and research facilities, due to its simplicity, repeatability, and direct force traceability. The calibration load cell serves as reference measurement, enabling characterization of the thrust measurement load cell response under controlled loading conditions. Calibration tests account for structural compliance, off-axis effects, and flexure stiffness. By comparing applied calibration forces to measure thrust signals, correction factors can be established and uncertainty quantified. This system allows routine pre-test and post-test calibration checks, ensuring measurement accuracy and reliability throughout test campaigns.

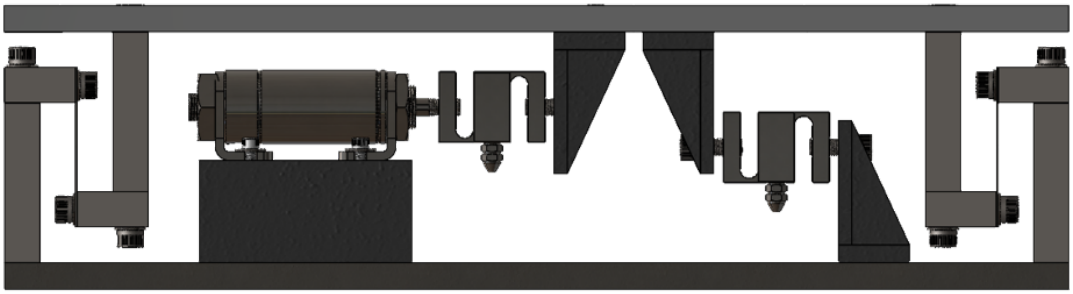

Fig. 11 FLARE test stand upper assembly.

5. Structural Analysis & Safety Margins

As mentioned, the student-designed, student-manufactured test stand structure is capable of withstanding loads up to 1500 lbf with a factor of safety of 4. The design employs vertically-oriented flexures to enable the top of the stand to float relative to the base, which enables translation in the thrust plane and thus force transmission into the load cell for thrust measurement. This flexure-based approach [20] eliminates issues faced in roller-based systems—e.g., static friction, bearing lubrication, track misalignment—and improves the load cell response/measurement fidelity under test conditions. The test stand structure is shown in Fig. 24.

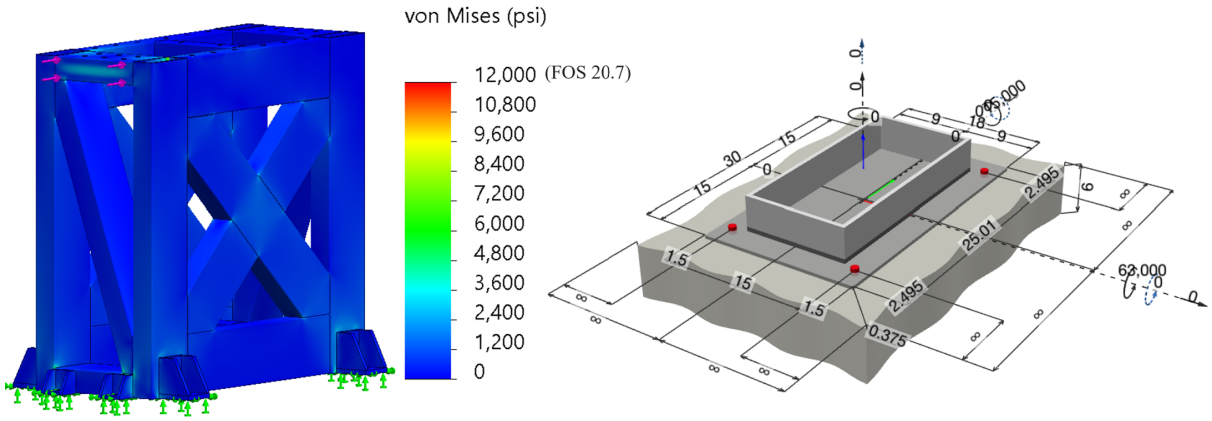

Fig. 12 Base structure simulation study

A calibration load cell is included with a pneumatic cylinder to provide reference values for the thrust measurements. Special attention was paid to enhancing the rigidity of all load-bearing members around critical load measurement

interfaces; deflection of load-bearing elements were calculated to assess impact on thrust measurement readings and part thicknesses were sized accordingly.

The base of the stand is constructed from square and rectangular steel tubing and components were full-penetration tungsten inert gas (TIG) welded in-house. The top plate and brackets/attachment components were machined at the UT San Antonio Makerspace machine shop and then fastened together. Analysis of the base structure was carried out to verify load-carrying capability and confirm that the factor of safety met established design constraints. Finite element simulation results in Fig. 12 indicate a maximum stress of approximately 12,000 psi, under the applied loading conditions of 6,000 lbf. Based on material yield strength of 62,000 psi, as specified by the material vendor, the resulting factor of safety is approximately 5.2. When referenced to the nominal operating load of 1,500 lbf, this corresponds to an effective overall safety margin of 20.7. This margin significantly exceeds the minimum design requirement of 4 and reflects conservative assumptions as well as appropriate design and material selection for the test stand.

An anchor analysis was performed to verify the structural adequacy of the substrate under expected thrust loading conditions. The test stand was mounted to an existing reinforced concrete slab with a thickness of 6 in, conservatively modeled as cracked concrete to account for potential service-level cracking. Loads are transferred into the concrete through anchor feet fabricated from ASTM A36 steel plate and post-installed adhesive anchors.

Anchoring is achieved using Hilti HIT-RE 500 V3 epoxy with 7/8 in diameter anchors embedded to a depth of 4 in., consistent with the recommendation from manufacturer analysis for structural anchorage in concrete.

Case	Thrust (lbf)	Concrete Strength (psi)	Concrete Condition	Concrete Breakout	Pryout	Combination
1	1500	2500	cracked	51%	5%	33%
2	6000	2500	cracked	151%	16%	139%
3	1500	5000	uncracked	27%	4%	12%
4	6000	5000	uncracked	94%	15%	91%

Table 3 Substrate analysis under different material and performance conditions.

While the cracked concrete assumption provides a conservative worst-case scenario estimate, realistically the concrete slab is expected to exhibit more favorable material properties. The slab was poured within the past five years as part of a new building installation and therefore representative of higher-strength concrete with no visible cracking in the anchoring region. Treating the slab as uncracked concrete is therefore more justified for a more realistic assessment of in-service performance.

Results from the refined analysis, summarized in Table 3, indicated that the resulting FOS exceeds 4 under the expected loading conditions. This margin provides confidence that the anchoring system meets performance requirements and ensures safe operation of the test stand.

D. Data Acquisition and Control

The FLARE data acquisition (DAQ) and control system enables deterministic control and robust sensor logging at sample rates >2 kHz, critical for capturing transient combustion events.

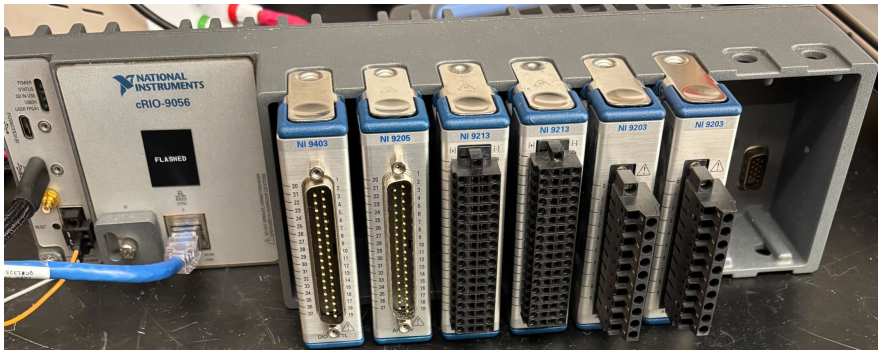

Fig. 13 cRIO-9056 used for DAQ/Control

A National Instruments (NI) compact real-time I/O controller (cRIO 9056) is used as the primary DAQ. NI 9205 and NI 9403 modules, for 32 analog voltage inputs and 32 digital in/outs respectively, are used to for recording load cell/voltage-based sensor data and for relay/valve control. A total of 4 NI 9203 modules are used to interface up to 32 current-based pressure transducers; current-based pressure transducers (4–20mA) are used for built-in fault detection (i.e., 0 mA readings) alongside reduced errors from line losses or electromagnetic interference (EMI). 2 NI 9015 modules are used to interface up to 32 thermocouples (various types) for both propellant flow monitoring and calorimetry analysis. The cRIO 904x/905x systems enable the usage of the NI-DAQmx module, which allows user-developed code to interface with the controller.

Since the device is an NI cRIO rather than an NI cDAQ, the real-time operating system on the controller is used for launching the data acquisition program instead of via a host computer. For initial (version 0) FLARE setup, a LABVIEW program was developed to quickly interface with the real-time controller and enable valve control and sequencing for research goals. For future operations, the NI Linux Real-Time operating system on the controller is used to launch a local python-based program which calls a circular buffer (python or C). A remote procedure call (gRPC) framework is used to interface a user's computer with the cRIO buffer, enabling control and data visualization through a python graphical user interface (GUI). Further work will be conducted to interface the cRIO with external or network attached storage (NAS) devices, and to test the speed of the circular buffer/interface with the gRPC connection.

```
12  class RealTimeBuffer:  1 usage
13      def __init__(self, analog_channels=32, digital_channels=15, buffer_size=1000, sample_rate=1000):
23          self.analog_channels = analog_channels
24          self.digital_channels = digital_channels
25          self.buffer_size = buffer_size
26          self.sample_rate = sample_rate
27
28          self.analog_buffer = deque(maxlen=buffer_size)
29          self.digital_buffer = deque(maxlen=buffer_size)
30
31          self.running = False
32          self.task_ai = None
33          self.task_di = None
34          self.acquisition_thread = None
```

Fig. 14 Snippet of student-developed python program for running a circular buffer on the cRIO controller

E. Electronics

1. Architecture and Design Intent

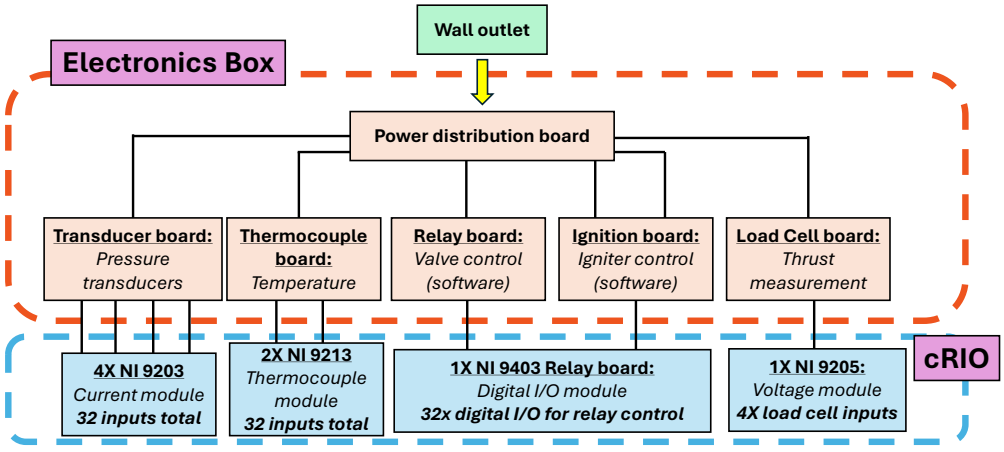

Fig. 15 Electronics architecture flow chart.

In-house electronics were built to handle FLARE operational demands in terms of both safety and modularity. Sensor counts, vibration demands, tolerance of components, and required degree of EMI/inductive voltage spike isolation—at a

student-accessible price range—demanded a custom, in-house solution. The following sections describe the custom printed circuit boards (PCBs)—power distribution board (PDB), transducer board (TB), thermocouple board (TCB), relay board (RB), ignition board (IB), and load cell board (LCB)—that were designed to interface with the NI cRIO modules and provide access to voltage-based sensors, current-based sensors, relays for valve control, and thermocouples. The electronics system architecture overview is shown in Fig. 15.

Modularity and failsafes were key design drivers to simplify debugging and maintenance during test campaigns. Critical sensors/control interfaces incorporate star grounding to avoid measurement errors and false triggering of relays through adjacent electronics. The printed circuit boards were designed in EasyEDA, SPICE simulations run in KiCAD, and components specified through JLCPCB.

2. Power Distribution Board

The power distribution board (PDB) provides conditioned power to each of the components within the electronics system. 24V and 12V AC/DC power supplies feed 8 and 6 independent outputs, respectively, and a 12V to 5V voltage regulator provides 5V power for 6 outputs. Switches are included for main power and independent output control. Embedded LED status lights are included for ease of use and diagnostics. The PDB design is shown in Fig. 16.

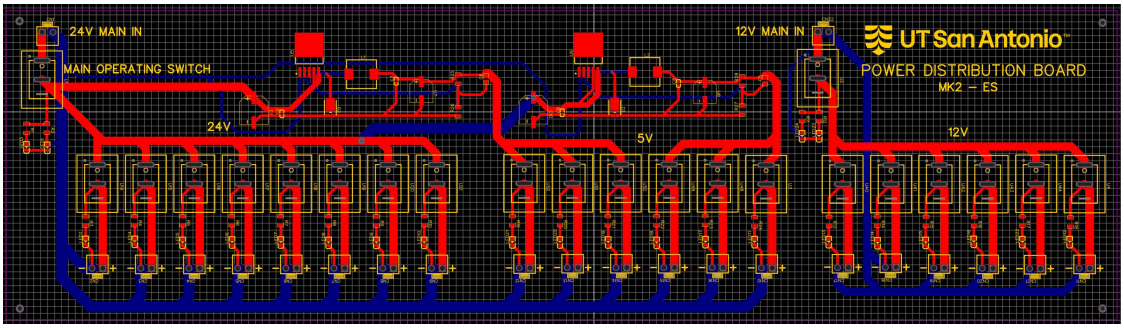

Fig. 16 Power Distribution Board design.

3. Transducer Board

The transducer board (TB) distributes 24V power to 16 current-based (4-20mA) pressure transducers and sends the transducer output signals to two D-subminiature (D-sub) DB9 connectors for delivery to 2 of the NI current input modules.

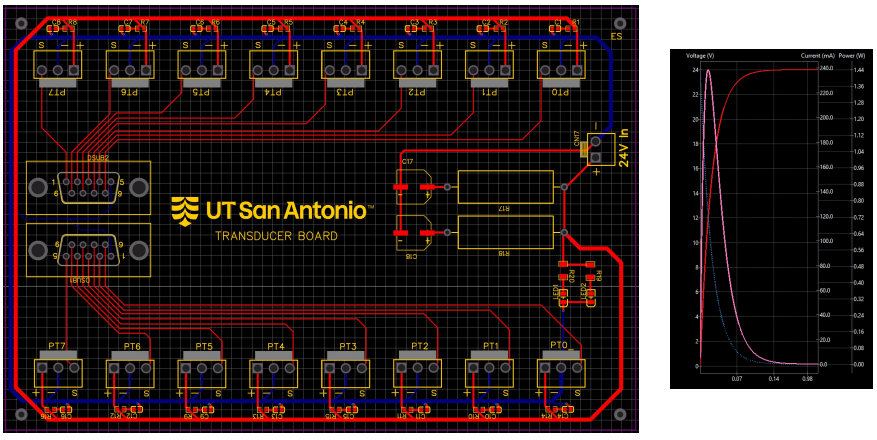

Fig. 17 Transducer board design and SPICE simulation of electrolytic capacitor section.

Bulk filtering of the inlet power is achieved by a resistor-capacitor (RC) circuit with electrolytic capacitors. This filtering minimizes noise in the excitation voltage supplied to the pressure transducers and reduces output signal error

(from noise), minimizing errors in pressure and thus flow rate measurements. A resistor and decoupling capacitor (ceramic) is used before the voltage excitation terminal on each transducer send to further suppress voltage fluctuations (high-frequency) for a clean power signal. The NI COM port connects via DB9 to the input power ground terminal. LEDs are included for confirmation of power. The TB design and SPICE simulation of the electrolytic capacitor section is shown in Fig. 17. A total of 2 transducer boards are used in the v0 facility setup.

4. Thermocouple Board

The thermocouple board (TCB) enables connection of 16 multi-type thermocouples for interface with the NI cRIO. T- and K-type thermocouples are used as the primary temperature measurement sensors for the v0 facility (different uncertainty ranges), and modularity included to enable E-type thermocouples in future system iterations. Fig. 18 shows the thermocouple board design. 2 TCBs are used in the v0 system.

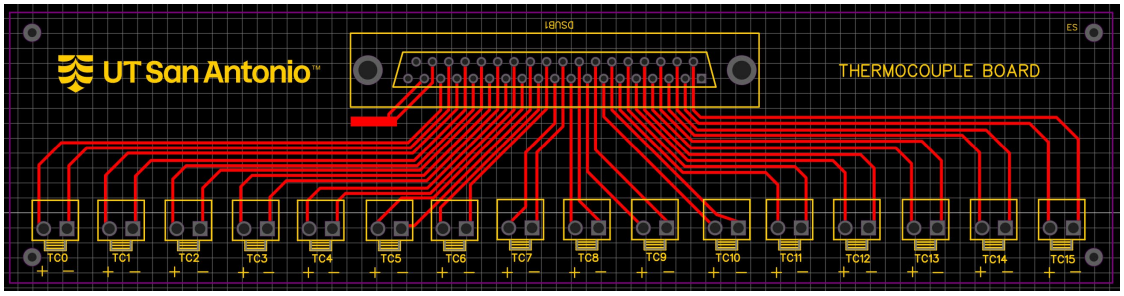

Fig. 18 Thermocouple board design.

5. Relay Board

The relay board controls valve logic for all facility flow operations. 5V logic-level signals are generated by the NI 9403 module and are received through the DB37 connector on the PCB. As the NI module cannot send enough current to reliably trip the relay, the 5V signal controls a MOSFET which enables a separate power source to control relay operation. After relay open, 24V, 12V, and 5V power are each sent through the relays to solenoid valves which supply pneumatics to each of the large pneumatic ball valves (propellant isolation and run). Flyback diodes are included in each relay circuit to mitigate inductive spikes (which could lead to consequences for other relays on the ground return path) and local filtering is incorporated to minimize noise issues near the MOSFET. A resistor is used as a "bleed orifice" (fluid analogy) to ensure the MOSFET can drain any accumulated charge (while it is closed) and mitigate misfires. Two AA batteries are included on an isolated circuit to power the barbecue igniter used for the propane flare system. A jumper is used to the ignition board for the ignition circuit on the ignition board. The relay board is shown in Fig. 19.

6. Ignition Board

The ignition board powers an automotive coil-on-plug (COP) ignition coil and uses a pulse width modulation (PWM) controller to supply a trigger signal to the COP transistor. This circuit is used to create repeatable sparks—with an automotive spark plug—suitable for torch igniter operation. This board uses a jumped signal from the relay board (from the NI 9403 5V logic). The ignition board is shown in Fig. 20.

7. Load Cell Board

The load cell board, also Fig. 20, uses a Texas Instruments amplifier and gain resistor to set maximum load cell output to 8V, chosen to measure load cell overages without clipping. Star grounding is used to isolate drain paths and provide more robust isolation for each attached load cell.

IV. Infrastructure Progress

This section briefly details the progress of the manufacturing and assembly of the facility as of December 2025, organized into different subsections by subsystem.

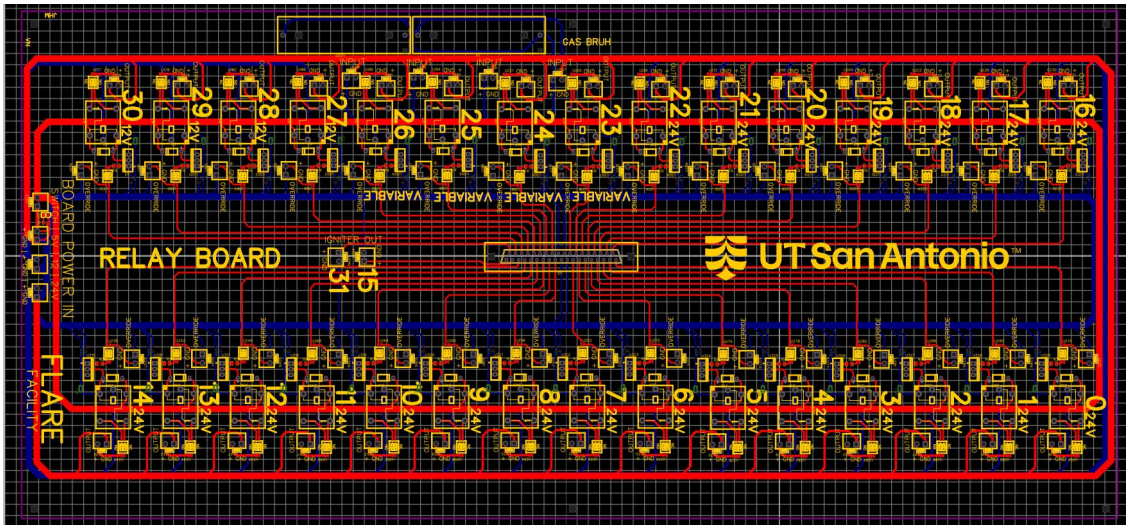

Fig. 19 Relay board design.

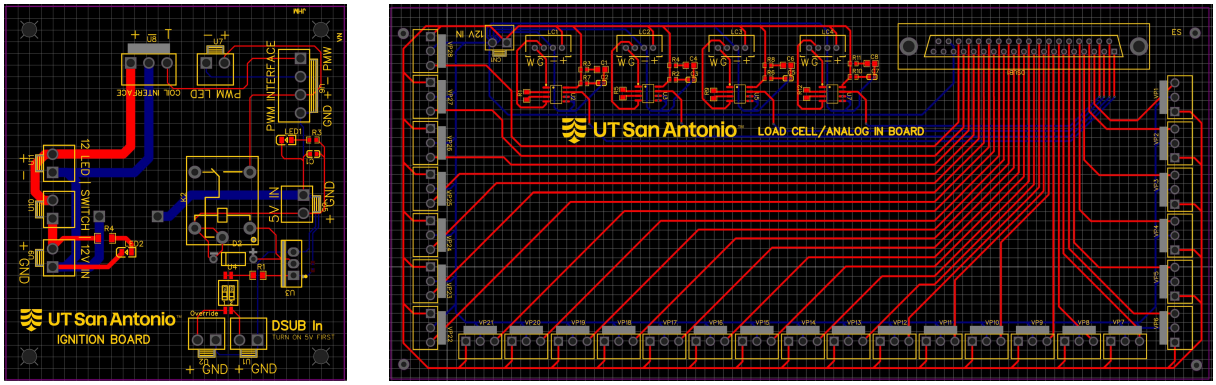

Fig. 20 Ignition board design *(left)* and load cell board design *(right)*

1. Coolant System

The water flow system comprises a water supply tank, water dump tank, and two 22 hp gasoline-powered pressure washer pumps from Canpump. These pumps (Model DBF-2821) provide a maximum pressure of 150 bar, a maximum flow rate of 52 LPM and require a power input of 18.5 kW. The pumps are powered by slightly different models of gasoline engines, one with a 678 cc displacement and the other with a 764 cc displacement, but both without built-in fuel containers. Appropriate fuel lines were identified and installed for each engine to operate on a gravity-fed system to provide fuel to the engine from above. Fuel stabilizers are used to mitigate the degradation of the gasoline during storage—the FLARE facility will potentially have much more downtime than a typical use-case for the gasoline engines.

Initial efforts involved identifying and sourcing the required inlet plumbing components, including fittings, adapters, and hoses necessary to support system operation. Several critical components were not readily available and were obtained through local donations or targeted procurement, including specialized fittings and hoses.

The cooling system uses 275 gallon IBC tanks (intermediate bulk container) and sourced from a local sponsor. Previously, these IBCs served as soap-carrying tanks. As a result, students thoroughly washed and cleaned them in preparation for water storage and handling. The sizes and configurations of the tanks are important to the run time. Notably, a reservoir connected to a single pump would empty in approximately 18 minutes (non-conservative estimation), and—in the case of two pumps connected to a single reservoir—less than 9 minutes. The pressure washer pumps were mounted onto carts and flow tested at the university to confirm operation. With respect to the water supply, water hardness is a major concern for the central Texas community, since it the buildup of scale tends to clog plumbing systems over time. As a result, water used for the system was evaluated using hardness test strips to detect calcium

and magnesium concentrations within a range of 0–425 ppm prior to circulation through the system. While additional filtration systems are intended to be used for preventative measures, the range of 0–25 ppm is considered appropriate for initial testing.

Progress of the construction, as of early December 2025, is shown in the photographs in Fig. 21.

Fig. 21 Coolant flow infrastructure, including water storage *(left)* and gasoline-powered pumps mounted on mobile carts *(right)*.

2. Test Stand Fabrication

The test stand is composed of three primary sections: substrate and anchoring system, the base structure, and the load assembly. The substrate and anchoring system encompass the interface between the reinforced concrete slab and the anchor feet attached to the base structure. The base structure forms the primary load-bearing truss of the test stand and provides the stiffness and rigidity required to withstand the extreme loading conditions expected during operation. The load assembly is the most complex section and consists of the hardware and instrumentation interfaces that enable test article integration and force measurement.

Base structure fabrication, as shown in Fig. 22, was conducted first and relied on innovative use of equipment available in the UT San Antonio machine shop. Rectangular and square tubing were initially cut slightly oversized and to the required angles using a horizontal bandsaw. The tubing was then faced on vertical milling machines to achieve dimensional accuracy, uniformity, and high-quality surface finishes. Following machining, the tubing was mounted on a table and V-grooves, consistent with the specified weld parameters, were ground into place. All components were then precisely fixtured on a welding table and tack welded. After verifying dimensional accuracy and alignment, all remaining welds were completed.

Fabrication of the load assembly, shown in Fig. 23, similarly utilized both the horizonal bandsaw and vertical milling machine to achieve precision and uniformity among the flexure system and load cell mounting components. In addition, a CNC mill was used to more accurately machine the base plate that interfaces the load assembly with the base structure, ensuring accurate bolt hole placement and component alignment. At the time of writing, the load assembly remains incomplete, with the test article fixture plate yet to be machined on the CNC mill.

Fig. 22 Photographs of the base structure fabrication process.

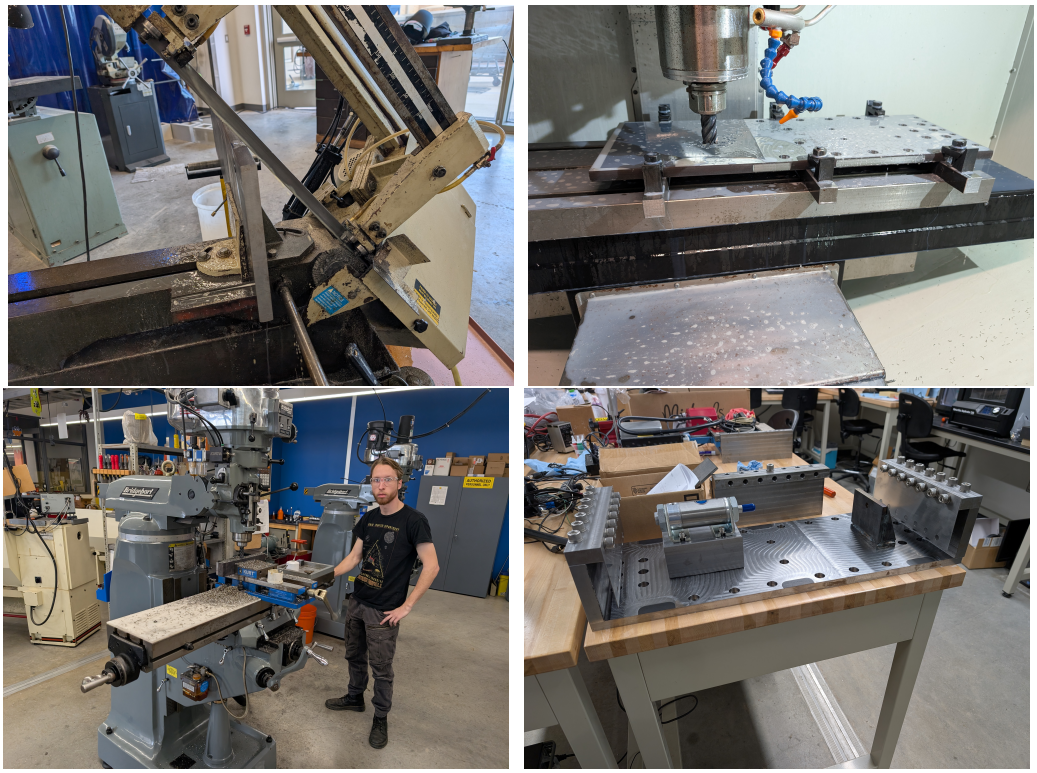

Fig. 23 Photographs of the load assembly fabrication process.

The substrate and anchoring system has yet to be installed: however, all required components are on hand and ready for integration. The remaining procedures include mounting hole preparation, anchor installation, and final mounting of the test stand. An SDS hammer drill will be used to bore mounting holes to the specified diameter and depth, followed by thorough cleaning to remove debris. Threaded rod will then be cut to length and mounted using a high-performance injectable epoxy mortar designed for structural steel anchorage. Finally, the test stand will be mounted using washers and nuts torqued to specification, with Belleville washers incorporated to reduce the likelihood of fastener loosening under dynamic loading.

Current fabrication state of the test stand structure, including weldment and custom machining of brackets and flexures with pneumatic cylinder installed, is shown in the photograph in Figs. 24.

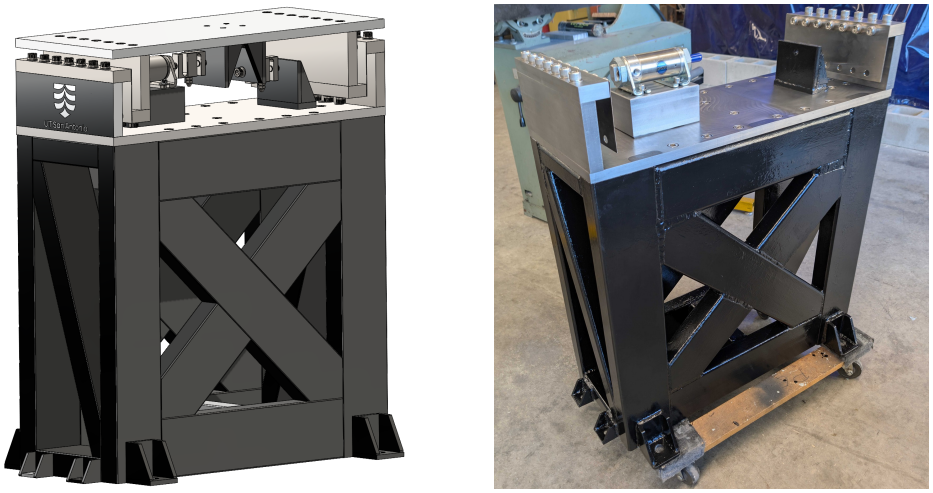

Fig. 24 Painted and assembled UT San Antonio FLARE test stand structure *(left)*, as-built *(right)*.

3. Propellant Fluid System

The propellant fluid delivery system, including regulators, pneumatically-actuated ball valves, pneumatic air supply control system, and overall plumbing is designed to be mounted on a mobile cart assembled from C-strut. To date, the mobile cart has been assembled, and several valves and fittings have been procured, as shown in Fig. 25.

Fig. 25 Fluid system CAD render *(left)*, stand structure *(middle)*, and valve hardware *(right)*.

Stainless steel tubing was used to fabricate multiple lengths of propellant lines, the the intended lengths shown in the left of Fig. 25. Both purge and fuel lines were cut, bent, and flared through an industry sponsor after providing raw materials. Flared tubing allows for AN fittings to be used throughout the system, which are advantageous for high fluid flow rates. The current tubing hardware, that has been cut, bent, and flared, is shown in Fig. 26.

The problem of gas cylinder storage for propellants was tackled through the conversion of locally-sourced bread carts into K-bottle 6 packs to enable cost-effective handling of 18 propellant bottles (six each for oxidizer, fuel, inert). The option to include up to six cylinders for each propellant type enables longer-duration hot-fire testing opportunities, which are a critical requirement for testing additively-manufactured thermal management strategies in propulsion systems. Additionally, the mobile configuration allows for modular and adaptable testing configurations, as well as security of the propellants (they can be stored inside when not in use). Photographs of the conversion process for the gas cylinder storage are shown in Fig. 28.

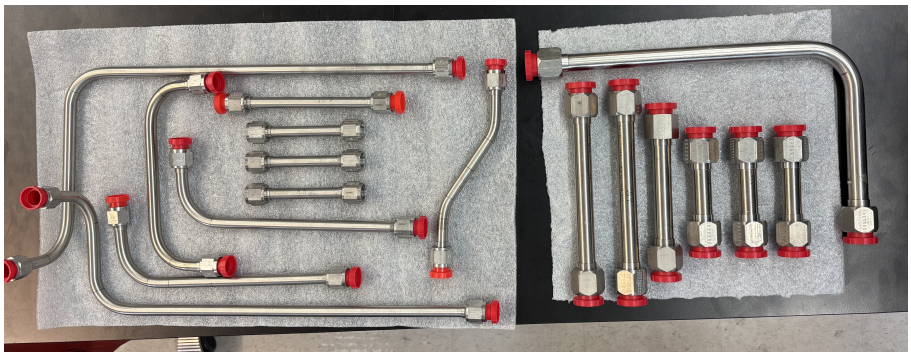

Fig. 26 Cut, bent, and flared tubing to be integrated into the fluid system.

Fig. 27 Conversion of bread carts to propellant K-bottle 6-packs

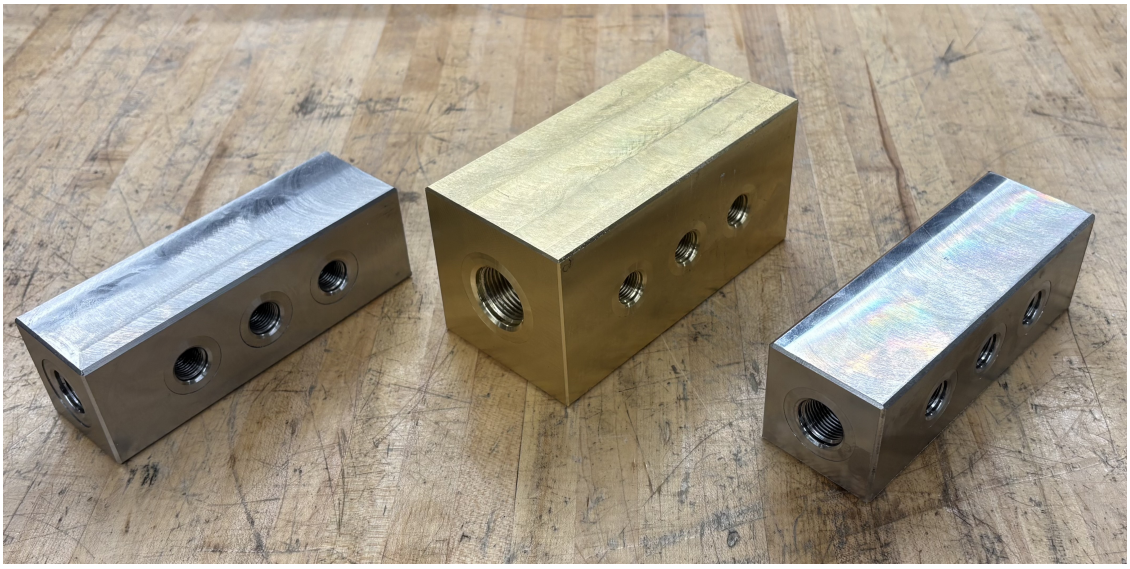

Fig. 28 Machined K-bottle 6-pack manifolds

4. Electronics

The completed in-house designed PCBs are shown in Fig. 29, and they are integrated into an enclosure box shown in Figs. 30, 31. At the time of writing, wiring is in progress to connect the different components and the relays will be tested in January 2026.

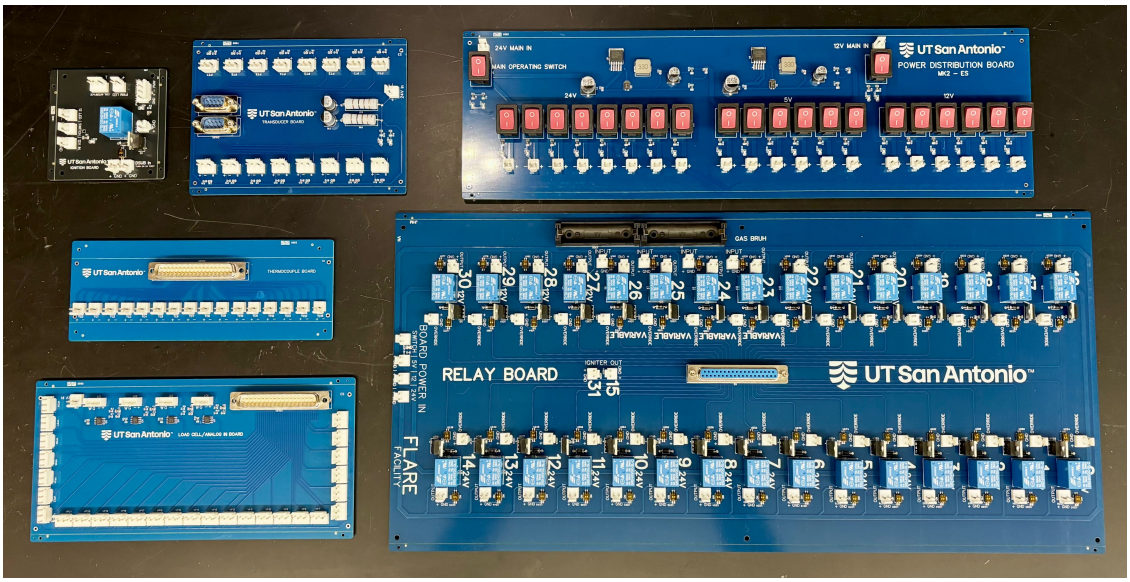

Fig. 29 Student-designed printed circuit boards (PCBs) for DAQ/control interface

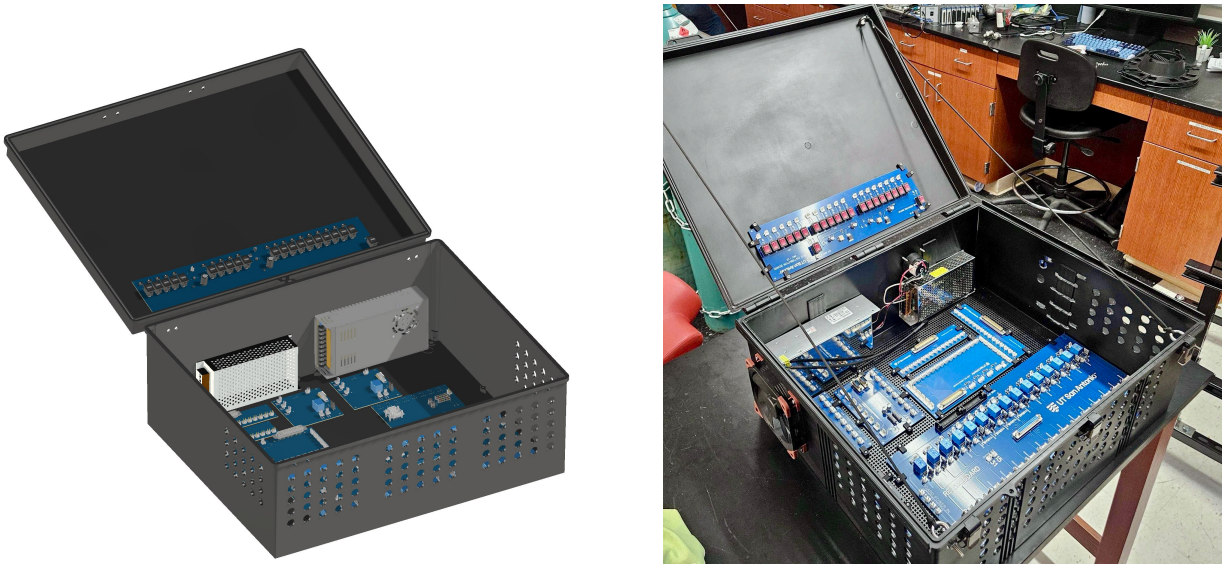

Fig. 30 CAD render of PCBs within electronics box *(left)*, as-built *(right)*

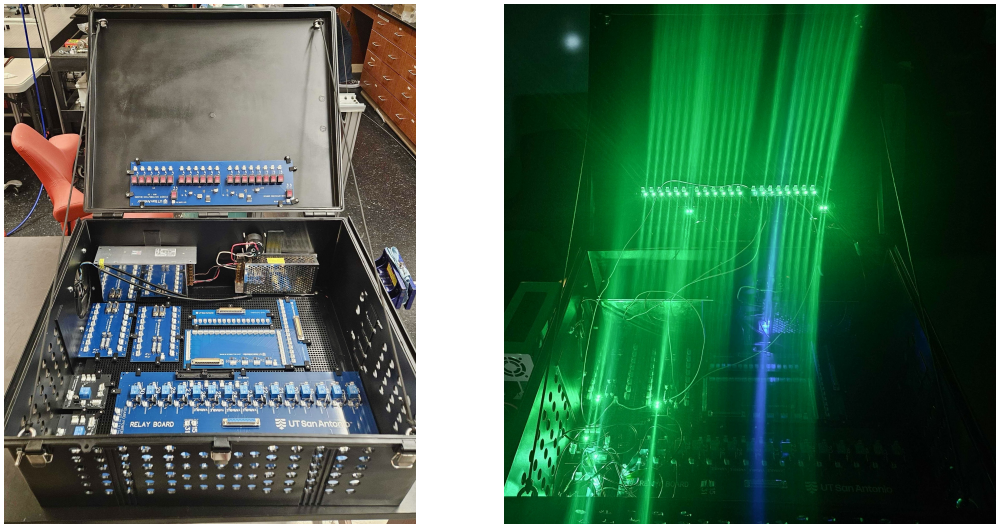

Fig. 31 Photograph of PCBs within electronics box as-built under high ambient lighting *(left)* and in low ambient lighting with indicator lights engaged *(right)*

5. Site Transformation

Lastly, the planned initial test site—behind dumpsters near the university machine shop—needed to be converted from a landfill to an operational propulsion test facility. As a combined effort, students cleared debris and swept the area. To confirm dimensions needed for hoses and properly depict the layout, the area was chalked and mapped. Bricks were acquired to protect existing walls from the generated fire plumes . These bricks were acquired through coordinated efforts involving students, alumni, and community members, including multiple trips to avoid vehicle overloading and damage. Cost savings were achieved by sourcing materials through local marketplaces and discounted listings. Future work includes painting.

Refurbishment efforts are shown in Fig. 32. Fig. 33 shows the cleaned up site as of October 2025 and its projected refurbishment in January 2026.

Fig. 32 Progress of site transformation on the UT San Antonio campus.

Fig. 33 Test site November 2025 *(left)*, projected view January 2026 *(right)*.

V. Future Work

December 2025 will be spent finalizing procurement of fittings and remaining plumbing hardware. System assembly, component/system-level checkouts, and full-system dry runs (i.e., sequence checkouts) will be conducted prior to test article integration. A deflagration-based propulsive test article will be additively manufactured at UT San Antonio as the first test article to qualify/de-risk the facility. Cold-flow testing, ox/fuel-blowdowns will be conducted to gather both propellant time of arrival (for sequence timers) and to determine dynamic pressure setpoints (i.e., regulator droop). Hot fire testing will be conducted in January 2026 and immediate follow-on testing will ensue for extreme environment materials research, optomechanical device development, and detonation heat transfer characterization.

Acknowledgments

This work is supported by a NASA Space Technology Graduate Research Opportunity (NSTGRO) award, Grant No. 80NSSC22K1215 and the AFRL-ML-RCP program, Award No. SPC-1000013908 GR 137103. J.H-M. is supported by a NASA Space Technology Graduate Research Opportunity (NSTGRO) award, Grant No. 80NSSC22K1215.

The authors thank Ari Goldman of Auburn University for critical insight into various components, manufacturers, cleaning procedures, and controls resources.

The authors wish to thank Isaac Esparza, Chris Ochoa, Scott Bourquin, Arturo Romero, Argyle Amberson, Kai Dennick, Amanda Lugo, Joshua Allen, Palak Patel, Aubrey Fuchs, Melaney Nickell, Ayden Lopez, Abrahim Galal, Enrique Alvarez, Makayla Watts, Nathan Hatch, and Alexander Schuleman for their assistance in manufacturing, welding, fabrication, assembly, and installation of various components.

The authors thank Thomas Teasley of NASA MSFC and Blaine Bigler of AFRL-EAFB for their support.

The authors thank Dr. Don Petersen and Dave Kuenstler for continued support of student-led fabrication efforts.

References

[1] Gradl, P. R., Mireles, O. R., Protz, C. S., and Garcia, C. P., *Metal Additive Manufacturing for Propulsion Applications*, Vol. 263, 2022. https://doi.org/10.2514/4.106279.

[2] Teasley, T., Petty, D., Skinner, S., and Hernandez-Mccloskey, J., "NASA'S COMPACT HIGH-EFFICIENCY ROTATING DETONATION ROCKET ENGINE FOR MARS INTERPLANETARY MISSIONS," *6th Annual AAS Guidance, Navigation and Control Conference*, 2024. URL https://ntrs.nasa.gov/citations/20240000933.

[3] Smallwood, J., "THERMAL AND STRUCTURAL CHARACTERIZATION OF A ROTATING DETONATION ROCKET ENGINE," Ph.D. thesis, Purdue University, 2024.

[4] Hernandez-Mccloskey, J., Reutlinger, S. A., Pineda, D. I., Teasley, T. W., and Petty, D. M., "Calorimeter Heat Flux Trends in NASA's Subscale Rotating Detonation Rocket Engine," *AIAA SciTech Forum*, 2025. https://doi.org/10.2514/6.2025-1979, URL http://arc.aiaa.org.

[5] Hernandez-McCloskey, J., Pineda, D. I., Bennewitz, J. W., Bigler, B. R., Burr, J. R., Danczyk, S. A., Paulson, E. J., and Hargus, W. A. J., "Design and analysis of an additively manufactured rotating detonation rocket engine chamber for calorimetry and thermal management assessment," *AIAA SciTech 2023 Forum*, 2023.

[6] Fetter, K. L., Steavenson, B., Donald, B., Andrade, A., Combs, C. S., Pineda, D. I., Burr, J. R., Bennewitz, J. W., and Bigler, B. R., "High-speed laser absorption measurements of temperature and carbon oxides in linear detonation channels," *AIAA AVIATION 2023 Forum*, American Institute of Aeronautics and Astronautics, Reston, Virginia, 2023. https://doi.org/10.2514/6.2023-4384, URL https://arc.aiaa.org/doi/10.2514/6.2023-4384.

[7] Hernandez-McCloskey, J., Nickell, M., Reutlinger, S., Eisenbarger, K., and Pineda, D. I., "Design of an Additively Manufactured Chamber for Combustion Health Monitoring in Air-Breathing Rotating Detonation Flows," American Institute of Aeronautics and Astronautics (AIAA), 2025. https://doi.org/10.2514/6.2025-3190.

[8] Fetter, K. L., Marquez, C. B., Ramirez, M. A., Marquez, B. N., Toby, J., Hernandez-McCloskey, J., and Pineda, D. I., "Design and construction of a modular thrust stand for propulsion research and education at UTSA," *AIAA Propulsion and Energy Forum*, Denver, CO, 2021.

[9] Toby, J. L., "Design and Performance Analysis of an Additively-Manufactured 316L Small-Scale Rocket Engine and Cooling Hardware," Ph.D. thesis, The University of Texas at San Antonio, 2023.

[10] Hernandez-McCloskey, J., and Pineda, D. I., "Laser absorption tomography of methane-oxygen flames in a metal additively manufactured torch ignition system," *40th International Symposium on Combustion*, Vol. Poster, Milan, IT, 2024.

[11] Petty, D., Teasley, T., Hernandez-Mccloskey, J., and Goldman, A., "Parameterized Study of Heat Load Trends in a Subscale Rotating Detonation Rocket Engine," *AIAA SciTech Forum*, 2025. https://doi.org/10.2514/6.2025-2150, URL http://arc.aiaa.org.

[12] Lightfoot, A., and Danczyk, S. A., "ACCURACY AND BEST PRACTICES FOR SMALL-SCALE ROCKET ENGINE TESTING," Tech. rep., 2011. URL https://apps.dtic.mil/sti/tr/pdf/ADA554591.pdf.

[13] NASA, "NASA ESDMD-001 - Moon to Mars Architecture Definition Document," Tech. rep., 2025. URL http://www.sti.nasa.gov.

[14] NASA, "NASA Moon-to-Mars Architecture - Mars Ascent Propellant Considerations," 2024.

[15] Bennewitz, J. W., Burr, J. R., Bigler, B. R., Burke, R. F., Lemcherfi, A., Mundt, T., Rezzag, T., Plaehn, E. W., Sosa, J., Walters, I. V., Schumaker, S. A., Ahmed, K. A., Slabaugh, C. D., Knowlen, C., and Jr, W. A. H., "Experimental validation of rotating detonation for rocket propulsion," *Scientific Reports*, 2023, pp. 1–13. https://doi.org/10.1038/s41598-023-40156-y, URL https://doi.org/10.1038/s41598-023-40156-y.

[16] The American Society of Mechanical Engineers, "ASME MFC-7-2016 - Measurement of Gas Flow by Means of Critical Flow Venturis and Critical Flow Nozzles," , 2021.

[17] Rathsack, T. C., Bigler, B. R., Bennewitz, J. W., Danczyk, S. A., and Hargus, W. A., "Laboratory flow measurement in rotating detonation rocket engines," *AIAA Scitech 2020 Forum*, Vol. 1 PartF, No. January, 2020, pp. 1–14. https://doi.org/10.2514/6.2020-0194.

[18] Majumdar, A. K., LeClair, A. C., Moore, R., and Schallhorn, P. A., "Generalized fluid system simulation program (GFSSP), version 6," *51st AIAA/SAE/ASEE Joint Propulsion Conference*, 2015, pp. 1–25. https://doi.org/10.2514/6.2015-3850.

[19] EIGA, "OXYGEN PIPELINE AND PIPING SYSTEMS - Doc 13/20," Tech. rep., 2020. URL www.eiga.eu.

[20] Runyan, R. B., Rynd, J. P., and Seely, J. F., "Thrust stand design principles," *AIAA 17th Aerospace Ground Testing Conference, 1992*, American Institute of Aeronautics and Astronautics Inc, AIAA, 1992. https://doi.org/10.2514/6.1992-3976.